ACS Sustainable Chemistry & Engineering

Research Article

pubs.acs.org/journal/ascecg

Facile Synthesis of Silver Nanoparticles Decorated Magnetic-Chitosan Microsphere for Efficient Removal of Dyes and Microbial Contaminants

Baskaran Ramalingam,[†] Md. Motiar R. Khan,[‡] Bholanath Mondal,[§] Asit Baran Mandal,[*,∥,⊥] and Sujoy K. Das[*,†,⊥]

[†]Bioproducts Laboratory, and [∥]Chemical Laboratory, Council of Scientific and Industrial Research (CSIR)−Central Leather Research Institute (CLRI), Chennai 600020, India

[‡]Department of Food Technology and Biochemical Engineering, Jadavpur University, Kolkata 700032, India

[§]Department of Central Scientific Service, Indian Association for the Cultivation of Science, Kolkata 700032, India

[⊥]Academy of Scientific and Innovative Research (AcSIR), New Delhi 110001, India

Supporting Information

ABSTRACT: A facile and rapid synthesis of core−shell type magnetite-chitosan microsphere decorated with silver nanoparticles (MCSM) is described. The composition and structure of the as-synthesized microsphere characterized by various spectroscopic and microscopic techniques demonstrated formation of 3.63 ± 0.76 μm MCSM with decoration of silver nanoparticles (AgNPs) having 16 ± 2.5 nm size. The thermogravimetric analysis (TGA) data showed good thermal stability, whereas vibrating sample magnetometry (VSM) analysis indicated the superparamagnetic behavior of the as-synthesized microsphere. The adsorptive removal and antimicrobial property of MCSM was explored for eco-friendly and cost-effective water purification. The MCSM removed 99.99% microbial contaminants and 99.5% of dyes from single as well as multicomponent systems from water bodies efficiently. Furthermore, the dye removal capacity of MCSM (q_e = 271.2 ± 14.5 mg/g) was found to be higher compared to the other nanoadsorbents attributing to the high effective surface area of the microsphere and plenty of functional groups of shell structure of chitosan favored binding of dyes on MCSM. Moreover, the adsorbed dyes were desorbed from MCSM at higher pH values and regenerated MCSM was used for next cycle of dye removal. The magnetic behavior of MCSM facilitated easy separation using external magnetic field leading to recycling and reuse, whereas decoration of AgNPs on the microsphere inhibited the bacterial growth. The long-term antibacterial activity of MCSM significantly improved the antifouling property to inhibit the biofilm formation on MCSM. The proposed core−shell type MCSM thus provides a promising opportunity for cost-effective water purification.

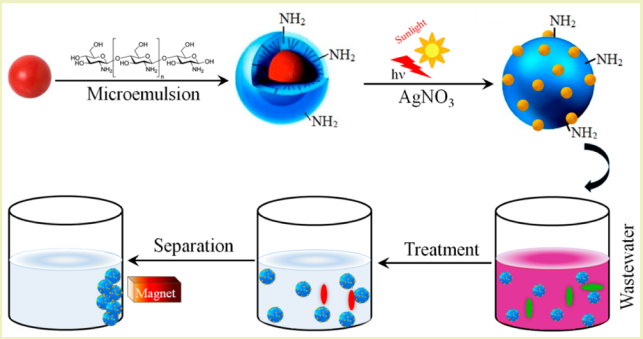

KEYWORDS: *Microsphere, Nanoadsorbent, Dye removal, Antibiofouling, Biofilm inhibition*

INTRODUCTION

Environmental pollution due to the disposal of large amounts of dye-bearing wastewater from the tannery, textile, paper and pulp industries is a global concern.[1,2] Most of these water-soluble dyes are nonbiodegradable and pollute both surface as well as groundwater causing serious threat to the aquatic and human life.[3,4] Microbial contamination of waterbodies further aggravates the problem for obtaining a safe, secure and sustainable source of water.[5,6] Thus, development of efficient treatment technology for removal of these pollutants is of paramount interest to control the water pollution and fulfill the ever increasing demand of sustainable water. Most of the common water treatment technologies such as membrane separation, solvent extraction, ion-exchange, adsorption, etc. are either energy intensive or restricted due to the high operational cost.[7−9] Moreover, the elimination of microbial contaminations requires continuous chemical treatments, like chlorination or ozone treatment, which often cause formation of harmful byproducts and raise health issues.[10,11] The development of alternative purification technology is therefore urgently required for effective separation and removal of water contaminants.[12]

The advances of nanoscience provide an opportunity to solve the technological constraint for the development of rapid,

Received: June 25, 2015
Revised: August 10, 2015
Published: August 17, 2015

DOI: 10.1021/acssuschemeng.5b00577
ACS Sustainable Chem. Eng. 2015, 3, 2291−2302

efficient and economically viable water purification technology. Nanostructured adsorbents,[4,5,13,14] nanofiltration membranes[15−18] and photocatalytic degradation and/or reduction[19,20] techniques have recently been demonstrated for the treatment of dye-bearing wastewater. Among them, nanoadsorbents are much more promising in water purification processes with the advantages of environmental benign route and cost-effectiveness. It has been observed that adsorption capacity increases significantly with decreasing size of the adsorbent to the nanoscale level. However, the nanoadsorbents suffer major draw backs due to the complicated and time-consuming separation process. In recent years, iron oxide nanoparticles have aroused considerable interest to address the environmental issues for their facile magnetic separation behavior, biocompatibility and large amount of surface reactive groups.[21,22] Various nanostructured iron oxide materials have been employed for removal of dyes and metal ions from aqueous solution recently.[21−23] However, tendency of aggregation of iron oxide nanoparticles in aqueous solution, which reduces the effective surface area, limits their application.[24,25] In addition, nanoparticles are very prone to biofilm formation in aqueous systems due to microbial growth on the surface of the nanomaterials.[26,27] The biofilm formation on the nanoparticles blocks the pore size and surface functional groups, thereby reducing the effectiveness of the nanoparticle. Simultaneously, development of antibiotic resistant strains creating serious health problem and economic loss.[28]

Tailoring the surface properties of iron oxide nanoparticle through functionalization with appropriate ligands or molecules is a very promising methodology for improving the stability, aggregation behavior and separation efficiency. Therefore, the current research focus has converged on the designing, synthesis and functionalization of the nanostructured iron oxide materials. Magnetic iron oxide nanoparticle fabricated using various inorganic as well as organic materials, such as multiwalled carbon nanotubes, porous carbon, manganese oxide, carboxyl groups, amine groups, and/or thiol groups, have been reported.[29−33] However, the functionalization of iron oxide nanoparticles is a very complicated process requiring prolonged time and sometimes damaging the magnetic structure including magnetic response. Significant improvement in the adsorption capacity is also a major challenge. Because the performance of nanomaterials in wastewater treatment depends on surface area and functional groups, the search for a suitable functionalization material is a continuing process. Chitosan, a potent natural biomaterial with abundant functional groups and tunable molecular structure, provides an opportunity for functionalization of iron oxide nanoparticles and designing a magnetically separable new functional nanomaterial.

Further, the wastewater treatment often runs long-term operation and thus requires stable and antifouling nanomaterials for preventing the biofilm formation. Because the silver nanoparticles (AgNPs) exhibit broad spectrum antimicrobial activity, decoration of AgNPs on magnetic-chitosan nanomaterial may lead to the formation of a novel antifouling nanomaterial.[34,35] Nevertheless, the formation of stable AgNPs requires flammable organic solvents and toxic reducing agents, which triggers environmental and safety issues.[36,37] Development of an environmentally benign facile synthesis process is thus a prerequisite to prepare silver nanoparticle decorated magnetic chitosan nanomaterial for cost-effective and efficient water purification. In this study, we developed a facile and environmental benign process to synthesize a core−shell magnetic chitosan microsphere decorated with silver nanoparticles (MCSM) as a smart antifouling nanomaterial for efficient removal of dyes and microbial contaminants from waterbodies for the first time. In the proposed core−shell type structure, the core and shell material acts independently. The inner magnetic core enables to separate the microsphere from the contaminated water; whereas the outer shell of AgNPs decorated chitosan helps to remove dyes and microbial contaminants and in addition prevents the bacterial growth on the surface of the nanomaterial. The multidye adsorbed capacity, antimicrobial, antifouling and magnetic separation properties of the proposed MCSM may provide a cost-effective water purification technology.

EXPERIMENTAL SECTION

Materials. Silver nitrate, Acid blue 113 (AB-113), Bromocresol green (BCG), Bromophenol blue (BPB), Congo red (CR), Eosine yellow (EY), Solochrome black (SB), Solochrome dark blue (SDB), Yellow 5GN (Y-5GN), Light liquid paraffin, Ferrous sulfate and all other chemicals were purchased from Merck, India and used as such without any further purification. The microbial media were procured from Hi-media, India. Chitosan (purity > 90%) was purchased from Bio Basic Inc., Canada.

Microorganisms. *Escherichia coli* (MTCC 062) and *Pseudomonas aeruginosa* (MTCC 424) used for the antimicrobial assays were obtained from the Institute of Microbial Technology, India and cultured in nutrient agar (0.3% beef extract, 0.5% peptone and 1.5% agar powder) slants and nutrient broth (0.3% beef extract and 0.5% peptone) as necessary.

Preparation of Dye Solution. Stock solutions (2000 mg/L) of different dyes (purity > 80%) viz. AB-113, BCG, BPB, CR, EY, SB, SDB and Y-5GN were prepared in deionized and double distilled water. The calibration curves of dye solutions were prepared by measuring absorbance of different concentrations of dyes with a UV−vis spectrophotometer (JASCO V650). The dye concentrations in the experimental samples were calculated from the calibration curves. A mixed dye solution was prepared by mixing all eight dyes in deionized and distilled water and maximum absorbance was recorded by scanning the dye solution in the UV−vis spectrophotometer. The calibration curve of the mixed dye solution was prepared as described above.

Synthesis of Water-Soluble Iron Oxide Nanoparticles. The water-soluble citrate coated hydrophilic iron oxide nanoparticles were prepared following the protocol of Hui et al.[38] In brief, sodium citrate (1 mmol), sodium hydroxide (4 mmol) and sodium nitrate (0.2 mol) were mixed in 19 mL of deionized and double distilled water and kept stirring at 100 °C for 1 h to maintain the homogeneity. 1 mL of freshly prepared 2 M ferrous sulfate solution was then added into the mixture dropwise under stirring conditions, and the solution was incubated for 1 h at 100 °C. The mixture was then allowed to cool down naturally to room temperature (30 ± 2 °C) and the pH of the reaction medium was increased to 12.0 using 1 M NaOH solution. A black suspension of iron oxide was formed within a few minutes, which was then separated using an external magnet. The obtained iron oxide nanoparticles were washed several times with deionized and double distilled water to remove unreacted chemicals and then finally dried by lyophilization.

Synthesis of the Magnetic-Chitosan Microsphere. The magnetic-chitosan microsphere (MCM) was prepared by a water-in-oil emulsion method. Initially, 1% (w/v) chitosan solution was prepared by dissolving chitosan flakes in 1% (w/w) acetic acid solution under stirring at 1800 rpm for 12 h. The magnetic nanoparticles (0.5 mg dry weight) were solubilized in 200 μL of double distilled water by ultrasonication for 15 min and added into 5 mL of chitosan solution followed by incubation under stirring for 1 h at 30 °C. The magnetic-chitosan solution was then added dropwise (~1 mL/min) into 25 mL of light liquid paraffin containing 50 μL of Span-80 under stirring at 1800 rpm to form water-in-oil emulsion. Subsequently, 300 μL of 25% glutaraldehyde solution was added into the suspension in various time

DOI: 10.1021/acssuschemeng.5b00577
ACS Sustainable Chem. Eng. 2015, 3, 2291−2302

intervals of 15 to 45 min and continuously stirred for another 5 h at the same speed. The obtained microsphere was then separated from the emulsion by centrifugation at 14000 rpm for 20 min. The process of centrifugation was repeated several times for complete removal of oil. The pellet was collected and washed with double distilled water and ethanol repeatedly to remove residual paraffin oil and Span-80. Finally, the MCM was dried by lyophilization.

Synthesis of MCSM. The AgNPs were synthesized on the surface of MCM by sunlight induced reduction of silver ions. 2.5 mL of 1000 mg/mL silver nitrate solution was placed in 100 mL conical flasks and 50 mg of MCM powder was added followed by incubation for 1 h under stirring (120 rpm) for binding of silver ions on the surface of MCM. AgNPs were then synthesized by reduction of bound silver ions through exposure to sunlight for 240 min. The AgNPs decorated MCM was subsequently centrifuged at 14000 rpm for 20 min. The pellet was collected and washed with double distilled water several times to remove unreacted silver ions. Finally, the MCSM was dried by lyophilization.

Characterization of MCSM. The MCSM synthesized, as described above was characterized by several spectroscopic and microscopic techniques. The UV−vis spectra of pure chitosan, iron oxide nanoparticles, MCM and MCSM were recorded on a JASCO V650 UV−vis spectrophotometer. Prior to the analysis, iron oxide nanoparticles, MCM and MCSM were dispersed in double distilled water by ultrasonication for 20 min. The X-ray diffraction (XRD) and thermogravimetric analysis (TGA) of the samples were recorded on a Philips X-ray diffractometer at 0−80° with a Cu Kα source (λ = 1.54 Å) and SDT Q600 TA Instrument (New Castle, USA) from 25 to 900 °C with heating rate of 10 °C/min, respectively. Fourier transform infrared spectra of the samples were recorded on a PerkinElmer FTIR spectrometer (FTIR-MB3000) from 4000 to 500 cm^{-1} at a resolution of 4 cm^{-1}. For field emission scanning electron microscopy (FESEM) analysis, samples were prepared by drop casting the suspension of samples on aluminum foil and dried naturally. The images were recorded on the FESEM instrument (JEOL JSM 6700F) equipped with EDAX. The morphology of the MCSM along with distribution of the synthesized AgNPs was analyzed by high resolution transmission electron microscopy analysis (HRTEM, JEOL JEM 2010). The magnetic properties of iron oxide nanoparticles, MCM and MCSM were recorded on a vibrating sample magnetometry instrument (VSM, Lakeshore 7410) at room temperature. The VSM was calibrated using a standard reference of high purity nickel sphere. The magnetic hysteresis loop was obtained using external magnetic field. The surface charge of the samples was measured through ζ-potential analysis of sample suspension on a Malvern Zetasizer.

Removal of Dyes Using MCSM. The adsorptive removal of cationic and anionic dyes was carried out using MCSM. Prior to this study, MCSM powder (2 mg/mL) was placed in a 100 mL conical flask and 25 mL of deionized and double distilled water was added followed by sonication for 10 min. The pH value of the suspension was adjusted to 2.0−9.0 by addition of 1 M HCl or NaOH solution as required followed by incubation for 10 min under shaking (120 rpm) to condition the MCSM. Following incubation, MCSM was collected by magnetic separation and added into 25 mL of 50 mg/L AB-113, BPB, BCG, CR, EY, SB, SDB and Y-5GN solutions separately placed in different 100 mL Erlenmeyer flasks and incubated for 1 h under shaking (120 rpm) at 35 ± 2 °C. On completion of incubation, the dye solution was separated by holding an external magnet and concentration of the residual dye was measured spectrophotometrically described above. The control experiments were carried out without addition of MCSM. The amount of dye adsorbed by MCSM was calculated using the mass balance equation.[39] A multicomplex dye system was prepared by mixing different dyes and testing the adsorptive removal of these dyes using MCSM in a similar fashion, as described above. The rest of the work was carried out with this mixed dye solution unless otherwise stated. The effect of pH on the removal of mixed dye was performed using preconditioned MCSM at different pH values (2.0−9.0) using 50 mg/L mixed dye solution. The kinetic study was carried out at three different pH values (2.0, 4.0 and 8.0) using the same dye concentration. The equilibrium adsorption isotherm was conditioned at the optimum pH (4.0) and time (25 min), keeping the other conditions the same as described above. The removal efficiency (R, %), amount of dye adsorbed at time t (q_t, mg/g) and at equilibrium (q_e, mg/g) were calculated using the following equations:[40]

$$R = \frac{100(C_0 - C_e)}{C_0} \quad (1)$$

$$q_t = \frac{(C_0 - C_t)V}{M} \quad (2)$$

$$q_e = \frac{(C_0 - C_e)V}{M} \quad (3)$$

where C_0, C_t and C_e are the initial, at time t and equilibrium concentration of dye (mg/L), respectively; V is volume of the dye solution (L) and M is the weight of MCSM (mg).

Recycling of MCSM. After the dye adsorption experiment, the MCSM was separated from the treated water by holding an external magnet and washed with deionized and double distilled water. The dye loaded MCSM was collected in different conical flasks and treated separately with different pH (2.0−14.0) solution and various organic solvents such as acetone, ethanol and methanol. At the end of the incubation, MCSM was collected by magnetic separation and washed with double distilled water. The regenerated MCSM was then used for next cycle of dye removal study, as described above.

Bacterial Growth and Biofilm Inhibition Properties of MCSM. The bacterial growth inhibition property of MCSM was studied by turbidity measurement against *E. coli* and *P. aeruginosa*. The sterile MCSM (2 mg/mL) was added separately in sterile nutrient broth and inoculated with freshly grown *E. coli* and *P. aeruginosa*. The cultures were incubated at 37 °C under shaking (120 rpm) for different time intervals and growth kinetics of *E. coli* and *P. aeruginosa* were monitored spectrophotometrically at 600 nm. The control experiment was conducted with MCM. The bactericidal activity of MCSM was determined by a plate count method against *E. coli* and *P. aeruginosa*. Briefly, *E. coli* and *P. aeruginosa* were grown in nutrient broth under shaking (120 rpm) at 37 °C to an early stationary phase (i.e., 12 h). The cultures were harvested from the fermented broth by centrifugation (10000 rpm for 15 min) and resuspended in K-media (2.4 g KCl and 3.1 g NaCl per liter). The final concentration of the culture was maintained at 10^7 CFU/mL. 25 mL of these bacterial cells were then placed in different conical flasks and incubated with MCSM at 37 °C under shaking (120 rpm) for 5 h. The control experiments were conducted under identical conditions with addition of MCM. Aliquots were taken at the end of incubation and plated on nutrient agar plate, which was then incubated overnight at 37 °C to grow the bacteria. The number of viable cells was measured by counting the colony grew on the agar plates. The killing efficiency was determined as follows:

$$\text{killing efficiency (\%)} = \frac{N_{MCM} - N_{MCSM}}{N_{MCM}} \times 100 \quad (4)$$

where N_{MCM} and N_{MCSM} are the number of bacterial colonies grown in the presence of MCM and MCSM, respectively.

The biofilm inhibition property of MCSM was assayed using *P. aeruginosa* as a model organism. 25 mL of *P. aeruginosa* (10^7 CFU/mL) was placed in a 100 mL conical flask and 2 mg/mL each of MCM and MCSM was added separately, followed by addition of sterile glucose solution to make the final concentration of 0.1% of glucose. The flasks were then incubated at 37 °C for 24 h under static conditions. The media was removed after 24 h of incubation carefully and a fresh 25 mL of sterile nutrient broth was added into the flasks. In each alternative day, media was removed and spiked with fresh sterile media. This was continued up to 96 h. The growth of *P. aeruginosa* in the suspension was recorded spectrophotometrically as described above. At the end of incubation (48, 72 and 96 h), both MCM and MCSM were collected and washed with sterile double distilled water to remove loosely attached cells. The biofilm formation on the surface

DOI: 10.1021/acssuschemeng.5b00577
ACS Sustainable Chem. Eng. 2015, 3, 2291−2302

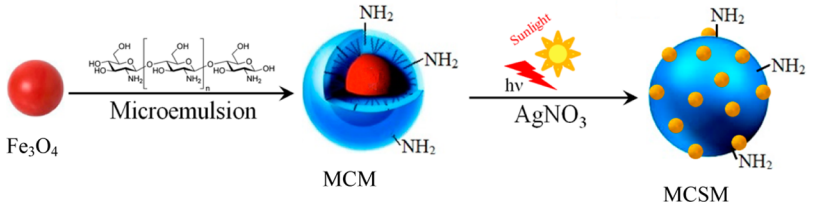

Figure 1. Schematic representation of the synthesis of silver nanoparticles decorated core−shell type magnetic-chitosan microsphere (MCSM).

of MCM and MCSM was then measured by crystal violet staining.[41] The adsorption of crystal violet on the pristine MCM and MCSM, without incubation with *P. aeruginosa*, was also recorded as control experiment. The cell viability of the biofilm was determined by staining with a live/dead viability kit (Invitogen, CA) and then fluorescent microscopic images were recorded on an Olympus BX-61 fluorescence microscope using an excitation filter of BP 460−495 nm and a band absorbance filter covering wavelengths below 505 nm. The structure of biofilm formation on MCM and MCSM was monitored by FESEM images. After 96 h of incubation, MCM and MCSM were washed with sterile phosphate buffer (50 mM, pH 7.2) and fixed with 2.5% glutaraldehyde solution in the same buffer followed by dehydration with graded ethanol series (40−100%). The samples were then dried and coated with gold. The micrographs were then recorded on the FESEM instrument operated at an accelerated voltage of 5 kV.

RESULTS AND DISCUSSION

Synthesis and Characterization of MCSM. The synthesis of MCSM is schematically presented in Figure 1, as described in the Experimental Section. Initially, water-soluble hydrophilic iron oxide nanoparticles were prepared by a coprecipitaion method in the presence of excess citrate along with nitrate ions[38] to distribute the negative charges evenly throughout the surface of the nanoparticles (ζ-potential −35.3 mV). This led to the formation of ∼28 nm magnetic nanoparticles (Supporting Information Figure S1) coated with citrate molecules. The as-prepared negatively charged magnetic nanoparticles were then allowed to bind electrostatically with positively charged chitosan (ζ-potential 16.5 ± 2.8 mV). The core−shell type magnetic-chitosan microsphere (MCM) was then prepared by the water-in-oil emulsion method, as described in the Experimental Section. In the process of preparation of MCM, the concentration of iron oxide nanoparticles was varied from 0.01 to 1% (w/v) with fixed concentration of chitosan (1%) solution. On the basis of the magnetic separation behavior and chitosan content, the addition of 0.1% iron oxide nanoparticles was found to be best for MCM (Figure S2) preparation. At higher concentrations of iron oxide nanoparticles, the chitosan content was low, and unsuitable for binding of dyes. On the other hand, at low concentrations of iron oxide nanoparticles, the microsphere was unable to separate from solution. The FTIR spectra were recorded to verify the encapsulation of iron oxide nanoparticles by chitosan and formation of MCM. The IR spectrum (Figure 2) of chitosan showed characteristic absorption bands at 3140 cm^{-1} due to −NH or −OH stretching vibrations and 3001 and 2884 cm^{-1} for −CH stretching of copolymer of chitosan, respectively. The amide I (C═O stretching vibration) and amide II (−NH bending and C—N stretching) appeared respectively, at 1635 and 1545 cm^{-1}. The absorption band at 1481 cm^{-1} was assigned to CH_2OH of C-6 position of the sugar moiety of chitosan.[42,43] The FTIR spectrum of iron oxide nanoparticles demonstrated peaks at 1682 and 1420 cm^{-1}, respectively due to the asymmetric and symmetric stretching vibration of the

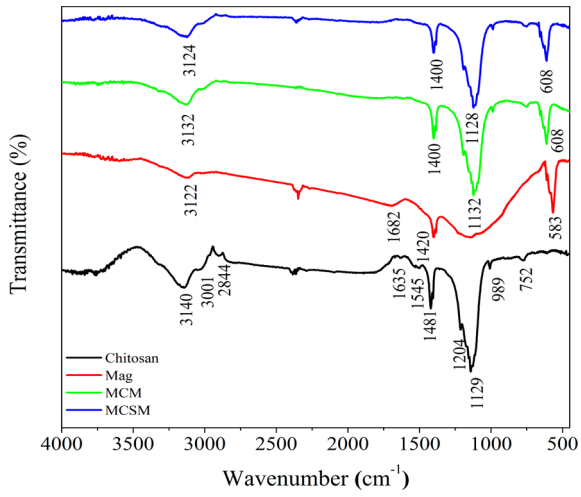

Figure 2. FTIR spectra of pure chitosan, citrate coated magnetic nanoparticles, MCM and MCSM.

$-COO^-$ group of surface coated citrate molecules. The peak of −CH stretching was also observed at 3122 cm^{-1}. The characteristic peak at 583 cm^{-1} corresponded to the Fe−O stretching vibration of iron oxide nanoparticles.[44] In the process of MCM preparation, the binding of iron oxide nanoparticles with chitosan resulted in weakening as well as shifting of −NH/OH stretching of the chitosan molecule. The band intensity at 3140 cm^{-1} was reduced, while −NH and/or −OH stretching of chitosan appeared at 3132 cm^{-1}. At the same time, the peaks of −CH stretching of chitosan disappeared in MCM. The corresponding conformational change of CH_2OH at C-6 was also envisaged by the appearance of new peak at 1400 cm^{-1}. In addition, disappearance of the amide I and amide II bands suggested binding of iron oxide nanoparticles to amine groups of chitosan. The cross-linking of amine group with glutaraldehyde in the formation of MCM might also be responsible for disappearance of amide bands. In addition, the $-COO^-$ stretching of surface carboxyl groups of magnetic nanoparticles also disappeared in MCM, while the Fe—O stretching vibration shifted to 608 cm^{-1}. The alterations of absorption bands therefore supported the coating of magnetic nanoparticles with chitosan forming MCM.

The decoration of AgNPs on the surface of MCM and subsequent formation of MCSM was carried out through sunlight induced reduction of surface bound silver ions (Ag^+). Following synthesis, MCM was treated with silver nitrate solution resulting in binding of positively charged Ag^+ ions on the surface of negatively charged MCM (−30.4 mV ζ-potential value). The surface bound Ag^+ ions were then reduced to AgNPs through exposure on sunlight leading to the formation of MCSM (Figure 3A). In the reaction medium, the dissolved oxygen reacted with the hydroxyl group of magnetic chitosan microsphere producing superoxide anion free radicals by UV

DOI: 10.1021/acssuschemeng.5b00577
ACS Sustainable Chem. Eng. 2015, 3, 2291−2302

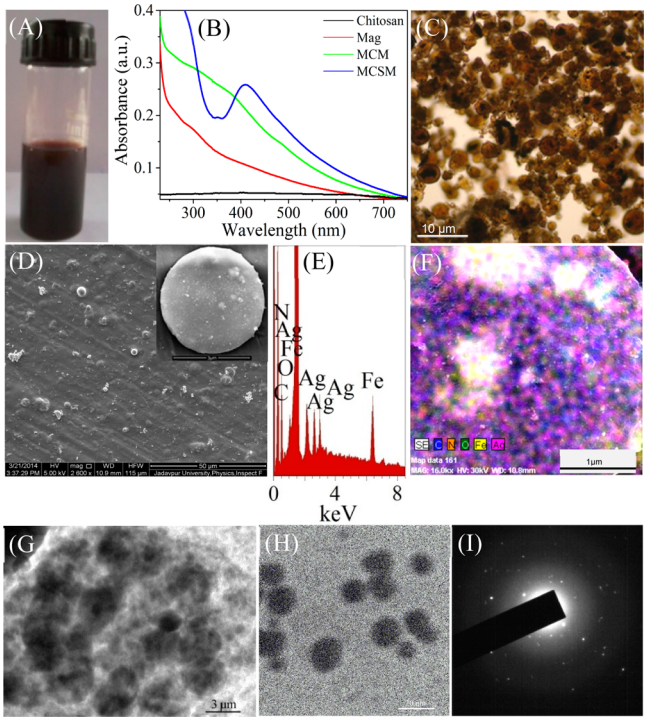

Figure 3. Color image (A); UV–vis spectra (B); optical microscopic image (C); FESEM image (D); EDXA spectrum (E); elemental mapping (F); TEM micrograph (G–H); high resolution image (H) of MCSM; selected area diffraction pattern (I) of AgNPs synthesized on MCSM. The inset picture in panel D shows the high resolution FESEM image of a single MCSM.

irradiation of sunlight and the generated superoxide anions induced reduction of Ag^+ ions into AgNPs possibly through the following steps:[45]

$$AgNO_3 \rightarrow Ag^+ + NO_3^-$$

$$Ag^+ + {}^-MCM \rightarrow Ag^+{-}MCM$$

$$MCM_{red} + O_2 \xrightarrow{\text{irradiation}} MCM_{OX} + O_2^{\cdot -}$$

$$O_2^{\cdot -} + Ag^+{-}MCM \xrightarrow{\text{reduction}} AgNPs{-}MCM\ (MCSM)$$

In the synthesis of AgNPs, the chitosan acted as a stabilizer and prevented the aggregation of AgNPs. Further, the synthetic process of MCSM did not require any reducing agent and organic solvent and thereby avoiding environmental contamination of toxic chemicals. The formation of AgNPs on the surface of MCM was subsequently characterized by UV–vis spectroscopy. The initial colorless solution of Ag^+ ions bound MCM turned sequentially light to dark brown within 4 h following exposure to sunlight with the appearance of a surface plasmon band of AgNPs at 410 nm (Figure 3B).[46] On the other hand, the UV–vis spectrum of magnetic nanoparticles and chitosan did not exhibit any such absorbance band. The Ag^+ ions treated MCM without exposure to sunlight did not demonstrate any SPR band of AgNPs even after incubation for 20 h, which clearly revealed reduction of Ag^+ ions to AgNPs induced by UV irradiation of sunlight. The FTIR spectrum of MCSM (Figure 2) further demonstrated the formation and stabilization of AgNPs. The initial incubation of Ag^+ ions with MCM caused rapid binding of positively charged Ag^+ ions on the electronegative (−30.4 mV ζ-potential value) surface and void of microsphere through hydroxyl and amine groups of chitosan, which resulted in shifting of the −NH/OH stretching band to 3124 cm^{-1}. However, the shifting of amide bands could not be detected due to very low intensities of amide bands in MCM. The formation of MCSM was further optimized by varying the sunlight exposure time. The kinetics of the reduction of Ag^+ to AgNPs was monitored spectrphotometrically following treatment of Ag^+ bound MCM under sunlight. The broad SPR band of AgNPs appeared at 390 nm with minimum exposure of 150 min and sharp peak appeared at 410 nm after exposure for 230 min only indicating nucleation and growth of AgNPs on MCM. However, further increase in exposure beyond 240 min caused broadening of SPR band might be due to the melting of AgNPs.

The size and shape of MCSM were determined by optical and scanning electron microscopies. Figure 3C shows a typical optical microscopic image of the as-prepared MCSM. A homogeneous distribution of monodisperse and spherical MCSM was distinctly observed in the image with size ranges from 2.8 to 4.2 μm. The histogram (Supporting Information Figure S3A) of the particle size distribution (n = 150) shows that average size of MCSM is 3.63 μm. Further structural information on MCSM was investigated by FESEM attached with EDXA. The low resolution FESEM image (Figure 3D) is very similar to that of the optical microscopic image with average diameter of 3.6 μm. The high resolution FESEM image of individual microsphere (Figure 3D, inset) clearly indicates the spherical shape of the microsphere having the diameter of 3.4 μm. The bright dots on the image also demonstrate the decoration of AgNPs on the surface of microsphere. The obtained AgNPs are clearly visualized by increasing the magnification of the FESEM image, as shown in the Supporting Information Figure S3B. The EDXA spectrum in Figure 3E clearly depicts the silver and iron peaks at 3 and 6 keV, respectively for AgNPs and Fe_3O_4. The C, N and O peaks in spectrum were originated from chitosan material of MCSM. The elemental mapping of MCSM presented in Figure 3F revealed the distribution patterns of C, N, O, Ag and Fe by different color codes. From this figure, the homogeneous decoration of AgNPs on the surface of the microsphere was clearly evidenced. The quantitative elemental analysis data further demonstrated that MCSM contained 8.3% (w/w) of Fe and 4.1% (w/w) of Ag. The TEM picture of the MCSM was also recorded to visualize the structure of the synthesized microsphere including dispersion and size of AgNPs on the MCSM. The image demonstrated the well dispersion of MCSM (Figure 3G) and further high resolution of the image clearly depicted the decoration of well dispersed spherical AgNPs (Figure 3H), with average size of 16 ± 2.5 nm, on the surface of the MCSM. The selected area electron diffraction (SAED) of AgNPs (Figure 3I) showed a Scherrer ring pattern associated with the [111], [200], [222] and [311] atomic planes of the face centered cubic (fcc) lattice of nanocrystalline AgNPs.[5]

Further confirmation of MCSM was carried out by XRD analysis. Figure 4A shows X-ray diffraction pattern of chitosan, magnetite, MCM and MCSM. The broad peak at 20° was attributed to the amorphous structure of chitosan, whereas the diffraction peaks of iron oxide nanoparticles appeared at 2θ values of 30, 35.4, 43, 53.4, 56.9 and 62.5° corresponded to [220], [311], [400], [422], [511] and [440] planes of cubic Fe_3O_4 lattice, respectively. As per the JCPDF data sheet (file no. 65-3107), these peaks indicated the cubic spinel structure of

DOI: 10.1021/acssuschemeng.5b00577
ACS Sustainable Chem. Eng. 2015, 3, 2291–2302

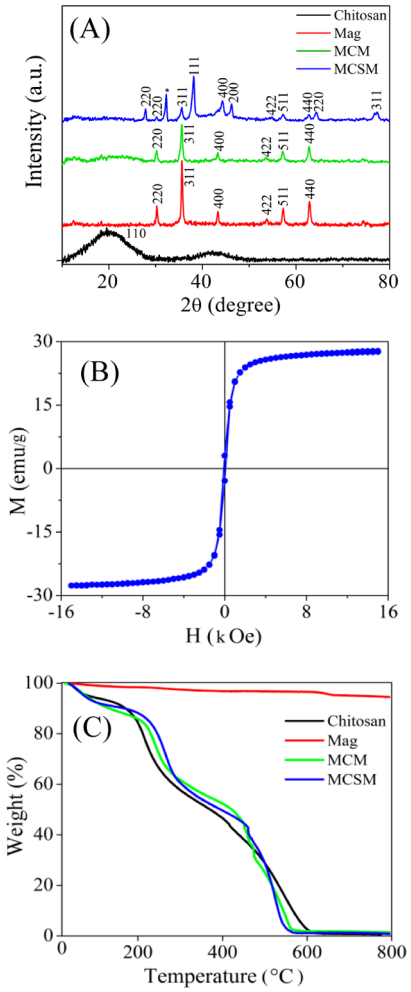

Figure 4. XRD (A); VSM (B); TGA of MCSM recorded at room temperature (C).

Fe_3O_4.[47,48] The XRD pattern of MCM showed strong diffraction peaks at 2θ values of 30, 35.4, 43, 53.4, 56.9 and 62.5° corresponding to the [220], [311], [400], [422], [511] and [440] planes of cubic Fe_3O_4 lattice and a weak diffraction peak of amorphous chitosan at 20°. The diffraction peak of chitosan was reduced due to binding of Fe_3O_4 in the chitosan matrix through the $-NH_2$/OH group of chitosan causing the disordered 3D crystal structure of chitosan.[49] The final MCSM exhibited additional peaks for the face-centered cubic structure of AgNPs (JCPDS file no. 4-0783)[50] along with a strong diffraction pattern of Fe_3O_4 and a weak peak of chitosan. The diffraction peaks of the [220], [111], [200], [220] and [311] planes of AgNPs appeared at 27.8, 38, 46, 64.5 and 77°, respectively. These results therefore clearly demonstrated that the crystal structures present in the MCSM had amorphous state of chitosan, and crystalline magnetite and AgNPs.

The magnetic property of MCSM was analyzed by VSM measurement at room temperature and demonstrated superparamagnetic behavior with S-shaped hysteresis loop (Figure 4B).[51,52] The saturation magnetization value of MCSM was found to be 27.6 emu/g, whereas the retentivity and coercivity values were 3.03 emu and 0.087 kOe, respectively. The hysteresis loop of control Fe_3O_4 nanoparticles showed the saturation magnetization value at 226.4 emu/g (Supporting Information Figure S4), whereas the retentivity and coercivity values were 24.2 emu and 0.088 kOe, respectively. Because the coercivity of MCSM and Fe_3O_4 nanoparticles remained the same and very close to zero, the MCSM formation did not reduce the superparamagnetic property of Fe_3O_4.[53] The low saturation magnetization of MCSM compared to the magnetite was attributed to the masking of Fe_3O_4 nanoparticles by thick layer of chitosan. However, the magnetism of MCSM is sufficient enough for magnetic separation of MCSM from the treated water by external magnetic field leading to easy recycling and reuse. The superparamagnetic behavior of MCSM thus prevented the aggregation of Fe_3O_4 nanoparticles and ensuring easy separation of microsphere by the external magnetic field.

The thermal stability of MCSM was studied by TGA. The thermogram of chitosan, magnetite, MCM and MCSM shown in Figure 4C shows the decomposition temperature of the samples. The TGA curve of Fe_3O_4 showed only 4% weight loss, resulting from evaporation of absorbed or crystalline water, for the whole temperature range. On the other hand, pure chitosan exhibited weight loss at three stages. The initial weight loss below 110 °C was quite small (8%) and corresponded to the removal of both adsorbed and bound water as well as residual acetic acid.[54,55] The second stage of weight loss of about 30% in the range of 180−350 °C was associated with the degradation and deacetylation of chitosan.[56] The complete degradation of chitosan started at 450 °C and ended at 600 °C. The preparation of MCM through incorporation of Fe_3O_4 into chitosan and subsequent formation of MCSM increased the stability of the compounds. Both MCM and MCSM demonstrated very similar thermogram patterns. Though the initial stage of water evaporation (7%) was same as that of chitosan, visible distinctions in the second and third stages of weight loss were observed. The MCM and MCSM started decomposition at 206 and 214 °C, respectively and ∼22% of weight loss was recorded at this stage. The final of decomposition started at 500 °C in both MCM and MCSM. Thus, TGA showed that the as-prepared MCSM has high thermal stability compared to the chitosan and very much suitable for the application in wastewater treatment.

Removal of Dyes by MCSM. The feasibility of the synthesized MCSM as a potential adsorbent for separation and removal of dyes (Figure 5A) was studied using commercially used eight different dyes including both cationic and anionic dyes. Figure 5B shows the color images of dyes before and after treatment with MCSM at low and high pH values. The percentage of dye adsorption at various pH values clearly depicted (Figure 5C) the pH dependent adsorptive behavior of MCSM toward AB-113, BCG, BPB, CR, EY, SB, SDB and Y-5GN. Almost 99% of anionic dyes (AB-113, BCG, CR, EY, SB, SDB, Y-5GN) was removed at an initial concentration of 50 mg/mL at a low pH range (2.0−4.0), whereas the cationic dye (BPB) was favorably removed at higher pH values, >8.0. The pH dependent adsorption property of MCSM suggested that electrostatic interaction played a significant role in the removal of anionic and cationic dyes. The shell structure of the core−shell type MCSM contained chitosan having $-NH_2$ and −OH functional groups, which could be easily protonated and deprotonated with alteration of pH values. To measure the surface charge of MCSM, ζ-potentials of the as-prepared MCSM were recorded at different pH values (2.0−8.0). At a low pH range (2.0−4.0), MCSM carried net positive charges (Supporting Information Table S1), which electrostatically attracted the negatively charged anionic dyes (AB-113, BCG, CR, EY, SB, SDB, Y-5GN). A similar phenomenon occurred at

DOI: 10.1021/acssuschemeng.5b00577
ACS Sustainable Chem. Eng. 2015, 3, 2291−2302

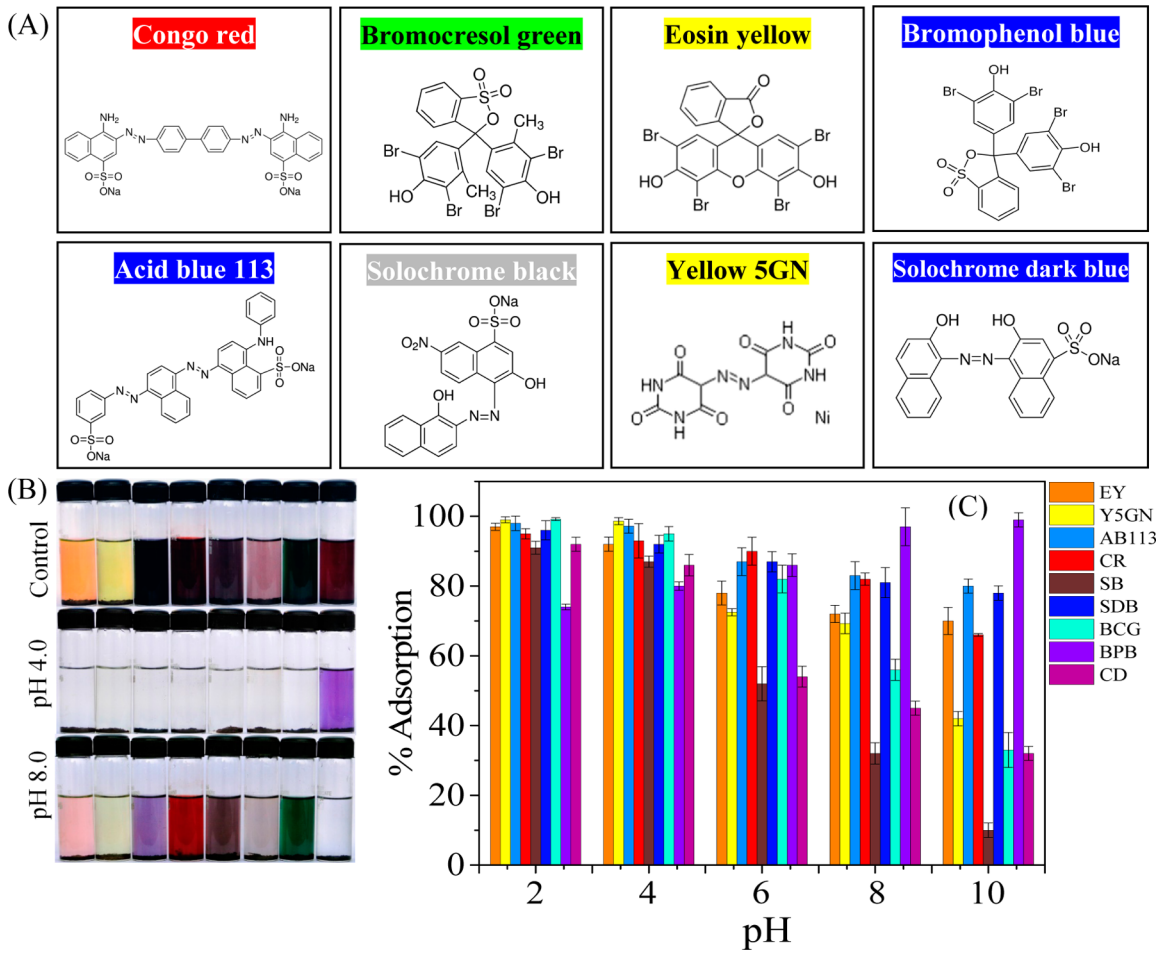

Figure 5. Chemical structures (A) of different anionic and cationic dyes (AB-113, BCG, BPB, CR, EY, SB, SDB and Y-5GN) used in the present study; color images (B) of dye solution before and after treatment with MCSM at two different pH values; percentages of dye adsorption (C) by MCSM at different pH values (2.0−10.0).

higher pH values (>8.0) for the cationic dye, where negatively charged MCSM attracted positively charged cationic dye (BPB). The pH dependent adsorption behavior of MCSM also demonstrated high stability of MCSM in a wide pH range and therefore has significant importance from practical viewpoints of wastewater treatment. Moreover, the MCSM could be easily and rapidly separated from aqueous solution following treatment with external magnetic field due to the superparamagnetic properties. The separated MCSM could also be redispersed in aqueous solution for further use once the applied magnetic field had been removed.

The effluents of dye-bearing wastewater often contain mixture of various kinds of dyes. Hence, it is highly necessary to investigate the adsorption capability of MCSM to treat the mixed dye solution. A cocktail dye (50 mg/mL) was prepared by mixing all eight dyes and adsorptive removal was carried out by measuring the absorption spectra of the dye solution after certain time intervals using 50 mg/mL of dye solution. The UV−vis spectrum of the control and treated dye presented in Figure 6A revealed the removal of multicomponent cocktail dye by MCSM. The absorbance maxima of the cocktail dye (blue line) diminished following treatment process (red line). The corresponding color image of the dye solution clearly depicted the removal of dyes (Figure 6A, inset) by MCSM and easy separation of MCSM from treated water by external magnetic field. The effect of pH and contact time was further optimized using the cocktail dye. The adsorptive removal of this dye was studied at three different pH values, i.e., 2.0, 4.0 and 8.0, by varying the contact time. Prior to this experiment, MCSM was initially conditioned at different pH values and then incubated with 50 mg/mL of cocktail dye solution for various time. Results show (Figure 6B) that dye was removed much effectively at low pH values, <4.0, and became completely colorless (Figure 6B, upper panel) within 25 min. It further showed that adsorptive removal was very fast at initial 5 min when 80% of dye was removed. Initially, the surface of MCSM contained abundant functional groups, which attracted the dye molecules. After the initial fast adsorption process, the binding occurred comparatively slowly and reached equilibrium within 25 min. The dye removal efficacy of MCSM (R = 99.48%) is much higher and faster than other reported adsorbents that required hours or even days to achieve satisfactory removal. The fast dye removal capacity of MCSM has significant practical importance for efficient treatment of water. To understand the dye binding process and rate controlling step, the kinetic data were fitted with different rate kinetic models and found that it followed the pseudo-second-order rate model (Figure 6C) very well (correlation coefficient 0.998) compared to the pseudo-first-order and intraparticle diffusion model (Supporting Information Table S2). Therefore, the rate-determining step occurred through a surface binding process, where most of the dyes adsorbed at the surface of MCSM. The

DOI: 10.1021/acssuschemeng.5b00577
ACS Sustainable Chem. Eng. 2015, 3, 2291−2302

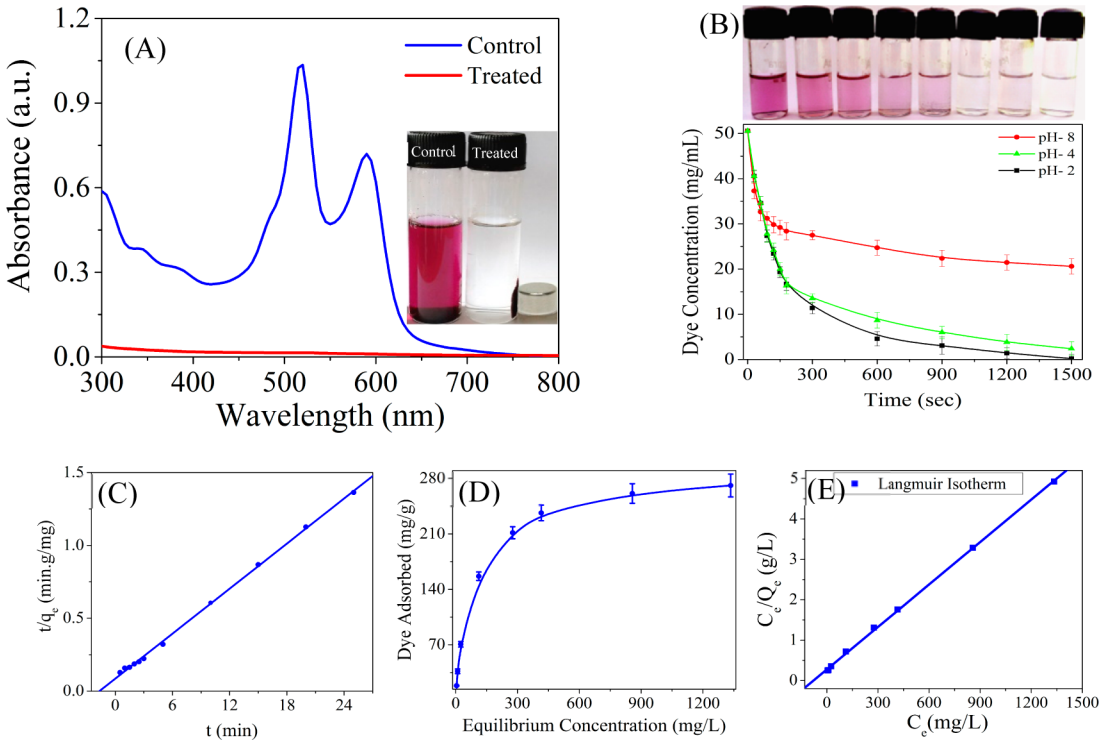

Figure 6. Removal of cocktail dye (A) by MCSM, inset picture shows the dye solution before and after treatment with MCSM; kinetics (B) of cocktail dye removal by MCSM, color image (upper panel) of dye removal at various time intervals; fitting of kinetics data (C) with pseudo-second-order rate model; adsorption isotherm (D) of cocktail dye on MCSM; fitting (E) of isotherm data with Langmuir model.

maximum adsorption capacity (Q_{max}) of MCSM was determined through equilibrium adsorption isotherm study (Figure 6D), which showed that the amount of dye adsorbed on MCSM increased with increase in dye concentration and finally attained equilibrium. The maximum dye adsorption capacity was found to be 271.2 ± 14.5 mg/g, which is 3 times higher than commercial activated carbon. Under similar conditions, activated carbon adsorbed 87.2 ± 5.6 mg/g of mixed dye. The adsorption capacity of MCSM was also found to be much higher in comparison to other adsorbents, as reported in the literature (Supporting Information Table S3).[57−65] For example, Fe_3O_4 nanoparticles adsorbed 67.1, 68.4, 37.7 and 44.4 mg/g, respectively of eriochrome black-T, bromophenol blue, bromocresol green and fluorescein,[57] $CeO_{2-\delta}$ nanopowder adsorbed 113, 101 and 91 mg/g of methyl orange, mordant blue 9 and reactive orange 16, respectively,[58] sawdust carbon and rice husk carbon powder adsorbed 183.8 and 86.9 mg/g of acid yellow 36 respectively,[59] $NiFe_2O_4$ adsorbed 47 mg/g of eriochrome black T[62] and cadmium hydroxide nanowire loaded on activated carbon adsorbed 108.7 mg/g of bromocresol green.[63] In spite of that, these adsorption studies were carried out in single dye system; whereas, in the present study MCSM removed dyes from multicomponent system and adsorbed 271.2 ± 14.5 mg/g of mixed dyes. The adsorption of dye in a single dye system is quite simpler than in a multicomponent dye system, where interaction occurrs in a more complex way. The high adsorption capacity and binding efficiency of MCSM toward a multicomponent dye solution is attributed to the high surface area of the microsphere and plenty of functional groups present on the chitosan shell of the core−shell type MCSM, which provides higher electrostatic attraction of dyes. The adsorption capacity of MCSM was also compared with chitosan, magnetite and magnetic-chitosan microsphere. We observed that Q_{max} of MCSM was quite high compared to chitosan (Q_{max} = 106 ± 18 mg/g at pH 5.5), and magnetite (Q_{max} = 62 ± 13 mg/g), that is almost equal to magnetic-chitosan microsphere (Q_{max} = 293 ± 15 mg/g) and cross-linked chitosan microsphere =308 ± 15 mg/g. It is worthwhile to mention here that the adsorption on surface depends both on surface area and surface functional groups. Fe_3O_4 nanoparticles though have high surface area but limited in surface functional groups. The chitosan has large number of functional groups, but has less surface area. The formation of microsphere therefore increased simultaneously the surface area as well as surface functional groups, which was reflected in high adsorption capacity of the microsphere. The low concentration of Fe_3O_4 (8.3% w/w) in the microsphere, however, enabled the microsphere to separate from solution by external magnetic field. In the same analogy, the formation of AgNPs on MCM reduced the adsorption capacity to a small extent.

The adsorption isotherm data was finally fitted with different isotherm models like Langmuir, Freundlich, Dubinin−Radushkevich and Temkin (Supporting Information Figure S4) to understand the interaction of dyes with MCSM at the surface binding process.[39] Figure 6E shows that Langmuir model obeyed perfectly with higher correlation coefficient (0.999). The theoretical monolayer saturation capacity of MCSM (276.9 ± 12.8 mg/g) calculated from Langmuir model matched very well with experimental values of 271.2 ± 14.5 mg/g, suggesting chemisorption and monolayer formation of dyes on MCSM. The multiplex dye adsorbability, stability in wide pH range, high adsorption capacity, fast kinetics and easy magnetic separation of MCSM is extremely useful for the treatment of multi dye containing wastewater.

DOI: 10.1021/acssuschemeng.5b00577
ACS Sustainable Chem. Eng. 2015, 3, 2291−2302

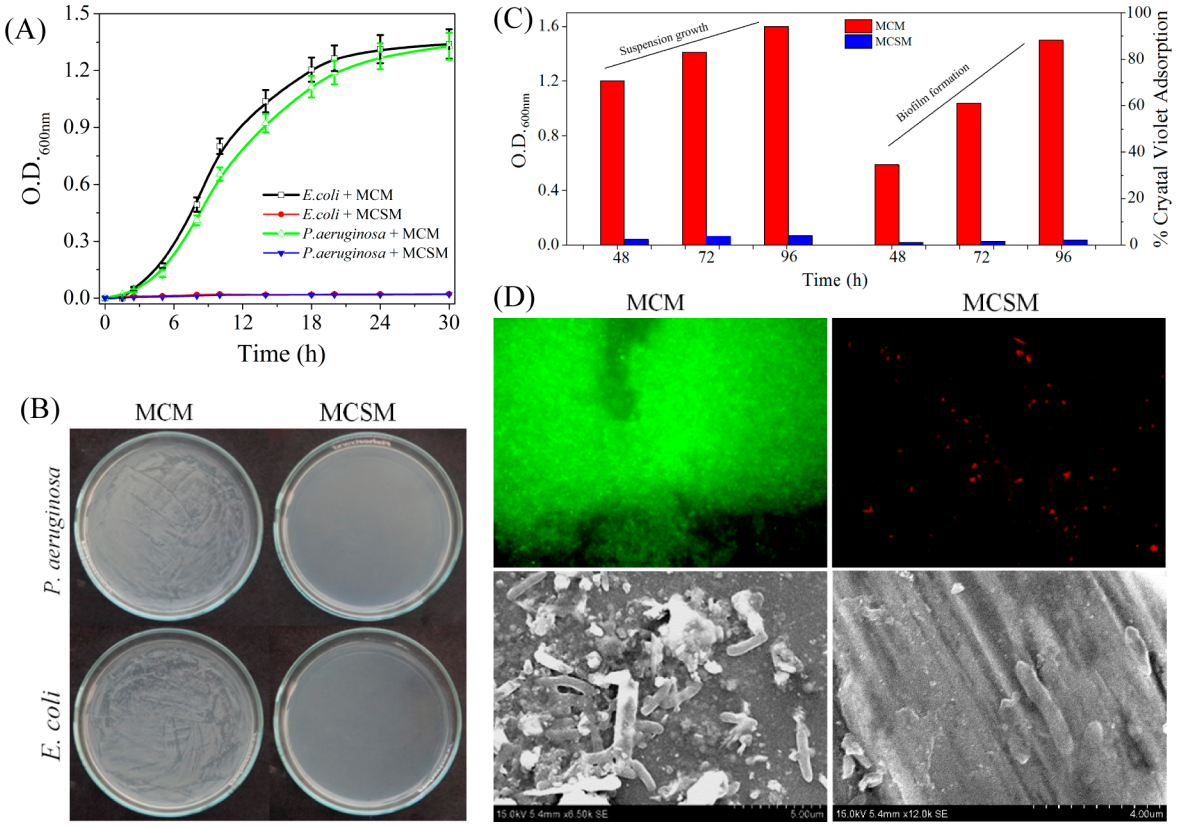

Figure 7. Growth kinetics of *E. coli* and *P. aeruginosa* (A) in nutrient broth containing 2.0 mg/mL of MCM and MCSM; antibacterial assay of MCM and MCSM against *E. coli* and *P. aeruginosa* by plate count method; bacterial growth in suspension and biofilm formation (C) on MCM and MCSM for various time intervals; analysis of biofilm structure (D) of *P. aeruginosa* on MCM and MCSM after 96 h of incubation, the green and red color in the fluorescence microscopic images (upper panel) indicates live and dead cells, respectively and FESEM image (lower panel) demonstrates structure of biofilm.

Desorption and Reuse of MCSM. Desorption of dyes from the dye adsorbed MCSM was studied to test the reusability of the microsphere. The MCSM was collected after dye adsorption, washed with distilled water to remove unbound dyes and then treated with various organic solvents and at different pH solutions. It was observed that with increasing the pH values of the eluent solution, the percentage of desorption was increased. At a higher pH value (14.0), more than 98% desorption of dyes was achieved. The electrostatic repulsion between the deprotonated dye molecules and negatively charged MCSM surface favored desorption of the dyes. The organic solvents were not so effective in the desoroption of dyes. Desorption of dyes at a higher pH value further proved the electrostatic interaction of dyes with MCSM. The multicyclic efficiency of MCSM was also examined by reusing the MCSM. In the first recycle process, MCSM adsorbed 99% of dyes and adsorbed 95% and 91% of dye respectively, in the second and third cycles of the operation. This clearly indicated reusability efficiency of MCSM in removal of dyes even in complex multicomponent dye system.

Inhibition of Bacterial Growth and Biofilm Formation. The wastewater always contains a large population of microorganisms, which often causes water borne diseases. Decontamination of wastewater is therefore an essential requirement for water purification. To eliminate the microbial contamination, wastewater undergoes chlorination or ozone treatment, but formation of toxic biproducts creates another health and environmental issues. The separate treatment process for removal of microbial contaminants also increases the cost of water purification. At the same time, the attachment and subsequent growth of microorganisms, present in the wastewater, frequently lead to the biofilm formation in treatment plant. This reduces the efficiency and increases the energy consumption, operational expenditure as well as accelerates corrosion formation in the treatment plant. Thus, reduction of microbial loads as well as prevention of biofilm formation is highly necessary for health and safety issues along with cost-effective water treatment. The bacterial growth inhibition property of MCSM was assayed against *E. coli* and *P. aeruginosa* by turbidity measurement. The nutrient broth supplemented with MCSM was incubated with *E. coli* and *P. aeruginosa* separately and growth of the organism was monitored spectrophotometrically at 600 nm through measuring the optical density. The control experiment was performed using MCM. The bacterial growth kinetics (Figure 7A) clearly showed that MCSM completely inhibited the growth of *E. coli* and *P. aeruginosa*. However, MCM failed to inhibit the bacterial growth under identical conditions, suggesting the antibacterial property of MCSM. The bactericidal activity of MCSM was further evaluated by a plate count method. Both *E. coli* (10^7 CFU/mL) and *P. aerugenosa* (10^7 CFU/mL) were treated with MCM and MCSM separately for 5 h and spread over the nutrient agar plates. Results depicted (Figure 7B) that bacterial colonies were not observed in the MCSM treated cells. In contrast, MCM treated cells showed dense growth of *E. coli* and *P. aeruginosa* colonies, which highlight the excellent bactericidal property of MCSM.

DOI: 10.1021/acssuschemeng.5b00577
ACS Sustainable Chem. Eng. 2015, 3, 2291−2302

At the end, the biofilm inhibition ability of MCSM was assessed against *P. aeruginosa* as a model organism. The biofilm formation of *P. aeruginosa* on MCSM and MCM was evaluated over a period of 96 h. Growth of the organism in the suspension as well as on the surface of the microsphere was recorded to measure the biofilm formation. The cell growth in suspension was monitored by recording the optical density on the UV−vis spectrophotometer, whereas the cell growth on the surface was measured through crystal violet staining. Initially, the freshly grown *P. aeruginosa* culture was treated with both MCM and MCSM separately and the biofilm of *P. aeruginosa* was allowed to grow on the microsphere surface for 96 h with continuous changes of media every alternate day. The growth of the organism in the suspension was recorded consecutively at 48, 72 and 96 h by measuring the absorbance at 600 nm (OD_{600}). It was observed that in MCM treated samples, the suspension became turbid following media change, but no visible cell growth was recorded in MCSM treated samples (Figure 7C). The MCM treated samples unable to prevent the growth of bacteria and the cells attached on the MCM grew with time leading to the formation of biofilm, which was later confirmed by staining the microsphere with crystal violet. The quantity of biofilm formation was represented by percentage of crystal violet adsorption. The result shows (Figure 7C) that a large amount of biofilm (high adsorption of crystal violet) was formed on MCM and with time the amount of biofilm was increased. In contrast, the biofilm formation was totally inhibited on MCSM. The result therefore clearly indicates that due to the strong antibacterial activity MCSM inhibited the growth of *P. aeruginosa* and prevented the biofilm formation. On the other hand, MCM was unable to prevent the bacterial growth; the attached cells grew with time resulting in the formation of complex biofilm structure. Thus, the decoration of AgNPs on the surface of MCM improved the long-term antibacterial activity and prevented the biofilm formation. The antibiofouling property of MCSM and cell viability in the biofilm structure of MCM was analyzed by live/dead assay. Figure 7D shows the representative fluorescence microscopic images of MCM and MCSM following staining of 96 h sample with live/dead viability kit containing SYTO 9 and propidium iodide (PI). The images clearly revealed that MCM was stained with bright green fluorescent color, which signified that thick layers of biofilm formed on MCM and cells were in live state. On the other hand, very few dead cells (red fluorescent color) were observed on MCSM, as PI specifically stains dead cells only and thus undoubtedly established the antibacterial and antibiofouling properties of MCSM. Finally, the biofilm structure and surface coverage was determined by FESEM analysis. Large population of healthy and rod shaped *P. aeruginosa* was observed in the biofilm structure developed on the entire surface of MCM (Figure 7D, lower panel, left). However, a very few scattered cells were noticed (marked by a circle in Figure 7D, lower panel, right) on the MCSM, indicating that *P. aeruginosa* could not survive to form the biofilm on MCSM. The image also showed the distorted and ruptured cells on the surface. The strong antibacterial activity and inhibition of biofilm formation on MCSM suggested that direct contact of AgNPs with bacteria caused rupture of the cell and ultimately prevented the bacterial growth on the MCSM surface. The antibacterial, antibiofouling and biofilm inhibition properties of MCSM would be beneficial for long-term treatment wastewater.

CONCLUSIONS

We have synthesized core−shell type MCSM, each with a magnetic core and chitosan shell decorated with AgNPs, for adsorptive removal of dyes and microbial contaminants from water for eco-friendly and cost-effective water purification. The magnetite chitosan microspheres displayed a spherical shape with AgNPs decorated on the surface of the microsphere. The MCSM showed a small hysteresis loop and low coercivity, indicating the superparamagnetic behavior of MCSM. The dye adsorption capacity of MCSM was found to be higher compared to the other adsorbents due to high surface area of the microsphere and large number of functional groups contained in the shell structure of chitosan. The dye binding process occurred through electrostatic interaction and perfectly obeyed the Langmuir model. MCSM also exhibited strong and long-term antibacterial activity against Gram-negative bacteria and prevented biofilm formation on the microsphere. The MCSM can be easily separated from treated water using an external magnetic field due to the magnetic core and regenerated by increasing pH values of the solution. We strongly believe that our protocol for the fabrication and application of MCSM in the removal of the dyes and microbial pathogens are very simple, convenient, cost-effective and environmentally sustainable for water purification.

ASSOCIATED CONTENT

Supporting Information

The Supporting Information is available free of charge on the ACS Publications website at DOI: 10.1021/acssuschemeng.5b00577.

Photograph and high magnified FESEM image of water-soluble citrate coated hydrophilic magnetite, photographs and optical microscopic image of the synthesized MCM, size distribution histogram and high magnified FESEM image of the asprepared MCSM, hysteresis loop of citrate coated magnetic nanoparticles measured at room temperature, fitting of adsorption isotherm data with Freundlich, Dubinin−Radushkevitch, and Temkin models, ζ-potential of MCSM conditioned at different pH values, parameters of rate kinetic models for adsorption of cocktail dyes on MCSM, summary of dye adsorption capacities of various adsorbents, adsorption isotherm study, and Langmuir, Freundlich, Dubinin−Radushkevich, and Temkin isotherm constants for adsorption of cocktail dyes on MCSM (PDF).

AUTHOR INFORMATION

Corresponding Authors

*S.K.D. E-mail: sujoy@clri.res.in; sujoydasiacs@gmail.com. Tel: +914424437133. Fax: +914424911589.

*A.B.M. E-mail: abmandal@hotmail.com; abmandal@clri.res.in. Tel: +914424910846. Fax: +914424912150.

Notes

The authors declare no competing financial interest.

ACKNOWLEDGMENTS

The authors gratefully acknowledge Department of Biotechnology and Council of Scientific and Industrial Research, Government of India for providing financial support under Rapid Grant for Young Investigators scheme (BT/PR6433/GBD/27/413/2012) and STRAIT programme, respectively.

DOI: 10.1021/acssuschemeng.5b00577
ACS Sustainable Chem. Eng. 2015, 3, 2291−2302

We also thank Prof. Lalitagauri Ray, Jadavpur University, Kolkata and Dr. T. Narasimhaswamy of Polymer Division, CLRI for providing ζ-potential measurement and optical microscopic facilities, respectively.

REFERENCES

(1) Soler, L.; Sánchez, S. Catalytic Nanomotors for Environmental Monitoring and Water Remediation. *Nanoscale* **2014**, *6*, 7175−7182.
(2) Parasuraman, D.; Serpe, M. J. Poly (N-Isopropylacrylamide) Microgels for Organic Dye Removal from Water. *ACS Appl. Mater. Interfaces* **2011**, *3*, 2732−2737.
(3) Lima, R. O. A. D.; Bazo, A. P.; Salvadori, D. M. F.; Rech, C. M.; Oliveira, D. D. P.; Umbuzeiro, G. D. A. Mutagenic and Carcinogenic Potential of a Textile Azo Dye Processing Plant Effluent that Impacts a Drinking Water Source. *Mutat. Res., Genet. Toxicol. Environ. Mutagen.* **2007**, *626*, 53−60.
(4) Xie, Y.; Yan, B.; Xu, H.; Chen, J.; Liu, Q.; Deng, Y.; Zeng, H. Highly Regenerable Mussel-Inspired Fe_3O_4@Polydopamine-Ag Core-Shell Microspheres as Catalyst and Adsorbent for Methylene Blue Removal. *ACS Appl. Mater. Interfaces* **2014**, *6*, 8845−8852.
(5) Das, S. K.; Khan, M. M. R.; Parandhaman, T.; Laffir, F.; Guha, A. K.; Sekaran, G.; Mandal, A. B. Nano-silica Fabricated with Silver Nanoparticles: Antifouling Adsorbent for Efficient Dye Removal, Effective Water Disinfection and Biofouling Control. *Nanoscale* **2013**, *5*, 5549−5560.
(6) Agnihotri, S.; Mukherji, S.; Mukherji, S. Size-controlled Silver Nanoparticles Synthesized Over the Range 5−100 nm using the Same Protocol and Their Antibacterial Efficacy. *RSC Adv.* **2014**, *4*, 3974−3983.
(7) Li, W.-W.; Yu, H.-Q.; He, Z. Towards Sustainable Wastewater Treatment by using Microbial Fuel Cells-Centered Technologies. *Energy Environ. Sci.* **2014**, *7*, 911−924.
(8) Khan, M. M. R.; Ray, M.; Guha, A. K. Mechanistic studies on the binding of Acid Yellow 99 on coir pith. *Bioresour. Technol.* **2011**, *102*, 2394−2399.
(9) Hao, N.; Jayawardana, K. W.; Chen, X.; Yan, M. One-Step Synthesis of Amine-Functionalized Hollow Mesoporous Silica Nanoparticle as Efficient Antibacterial and Anticancer Materials. *ACS Appl. Mater. Interfaces* **2015**, *7*, 1040−1045.
(10) Buffle, M. O.; Galli, S.; von Gunten, U. Enhanced Bromate Control during Ozonation: The Chlorine-Ammonia Process. *Environ. Sci. Technol.* **2004**, *38*, 5187−5195.
(11) Won, S. W.; Choi, S. B.; Chung, B. W.; Park, D.; Park, J. M.; Yun, Y.-S. Biosorptive Decolorization of Reactive Orange 16 using the Waste Biomass of *Corynebacterium glutamicum*. *Ind. Eng. Chem. Res.* **2004**, *43*, 7865−7869.
(12) Alonso, A.; Berbel, X. M.; Vigues, N.; Rodriguez, R. R.; Macanas, J.; Munoz, M.; Mas, J.; Muraviev, D. N. Superparamagnetic Ag@Co-Nanocomposites on Granulated Cation Exchange Polymeric Matrices with Enhanced Antibacterial Activity for the Environmentally Safe Purification of Water. *Adv. Funct. Mater.* **2013**, *23*, 2450−2458.
(13) Zhai, T.; Xie, S.; Lu, X.; Xiang, L.; Yu, M.; Li, W.; Liang, C.; Mo, C.; Zeng, F.; Luan, T.; Tong, Y. Porous $Pr(OH)_3$ Nanostructures as High-Efficiency Adsorbents for Dye Removal. *Langmuir* **2012**, *28*, 11078−11085.
(14) Gupta, S. S.; Sreeprasad, T. S.; Maliyekkal, S. M.; Das, S. K.; Pradeep, T. Graphene from Sugar and Its Application in Water Purification. *ACS Appl. Mater. Interfaces* **2012**, *4*, 4156−4163.
(15) Yu, L.; Zhang, Y.; Wang, Y.; Zhang, H.; Liu, J. High Flux, Positively Charged Loose Nanofiltration Membrane by Blending With Poly (Ionic Liquid) Brushes Grafted Silica Spheres. *J. Hazard. Mater.* **2015**, *287*, 373−383.
(16) Xing, L.; Guo, N.; Zhang, Y.; Zhang, H.; Liu, J. A Negatively Charged Loose Nanofiltration Membrane by Blending with Poly (Sodium 4-Styrene Sulphonate) Grafted SiO_2 via SI-ATRP for Dye Purification. *Sep. Purif. Technol.* **2015**, *146*, 50−59.
(17) Zhu, J.; Tian, M.; Zhang, Y.; Zhang, H.; Liu, J. Fabrication of a Novel "Loose" Nanofiltration Membrane by Facile Blending with Chitosan-Montmorillonite Nanosheets for Dye Purification. *Chem. Eng. J.* **2015**, *265*, 184−193.
(18) Zhu, J.; Zhang, Y.; Tian, M.; Liu, J. Fabrication of a Mixed Matrix Membrane with in Situ Synthesized Quaternized Polyethylenimine Nanoparticles for Dye Purification and Reuse. *ACS Sustainable Chem. Eng.* **2015**, *3*, 690−701.
(19) Yao, T.; Cui, T.; Wang, H.; Xu, L.; Cui, F.; Wu, J. A Simple Way to Prepare Au@polypyrrole/Fe_3O_4 Hollow Capsules with High Stability and Their Application in Catalytic Reduction of Methylene Blue Dye. *Nanoscale* **2014**, *6*, 7666−7674.
(20) Pegu, R.; Majumdar, K. J.; Talukdar, D. J.; Pratihar, S. Oxalate capped iron nanomaterial: from methylene blue degradation to bis(indolyl)methane synthesis. *RSC Adv.* **2014**, *4*, 33446−33456.
(21) Yuan, J.; Liu, X.; Akbulut, O.; Hu, J.; Suib, S. L.; Kong, J.; Stellacci, F. Superwetting Nanowire Membranes for Selective Absorption. *Nat. Nanotechnol.* **2008**, *3*, 332−336.
(22) Shannon, M. A.; Bohn, P. W.; Elimelech, M.; Georgiadis, J. G.; Mariñas, B. J.; Mayes, A. M. Science and Technology for Water Purification in the Coming Decades. *Nature* **2008**, *452*, 301−310.
(23) Xu, P.; Zeng, G. M.; Huang, D. L.; Feng, C. L.; Hu, S.; Zhao, M. H.; Lai, C.; Wei, Z.; Huang, C.; Xie, G. X.; Liu, Z. F. Use of Iron Oxide Nanomaterials in Wastewater Treatment: A Rev. *Sci. Total Environ.* **2012**, *424*, 1−10.
(24) Peik-See, T.; Pandikumar, A.; Ngee, L. H.; Ming, H. N.; Hua, C. C. Magnetically Separable Reduced Graphene Oxide/ Iron Oxide Nanocomposite Materials for Environmental Remediation. *Catal. Sci. Technol.* **2014**, *4*, 4396−4405.
(25) Wu, W.; He, Q.; Jiang, C. Magnetic Iron Oxide Nanoparticles: Synthesis and Surface Functionalization Strategies. *Nanoscale Res. Lett.* **2008**, *3*, 397−415.
(26) Borcherding, J.; Baltrusaitis, J.; Chen, H.; Stebounova, L.; Wu, C. M.; Rubasinghege, G.; Mudunkotuwa, I. A.; Caraballo, J. C.; Zabner, J.; Grassian, V. H.; Comellas, A. P. Iron Oxide Nanoparticles Induce *Pseudomonas aeruginosa* Growth, Induce Biofilm Formation, and Inhibit Antimicrobial Peptide Function. *Environ. Sci.: Nano* **2014**, *1*, 123−132.
(27) Toyofuku, M.; Roschitzki, B.; Riedel, K.; Eberl, L. Identification of Proteins Associated with the *Pseudomonas aeruginosa* Biofilm Extracellular Matrix. *J. Proteome Res.* **2012**, *11*, 4906−4915.
(28) Li, Y.; Ma, J.; Zhu, H.; Gao, X.; Dong, H.; Shi, D. Green Synthetic, Multifunctional Hybrid Micelles with Shell Embedded Magnetic Nanoparticles for Theranostic Applications. *ACS Appl. Mater. Interfaces* **2013**, *5*, 7227−7235.
(29) Hasegawa, R. Design and Fabrication of New Soft Magnetic Materials. *J. Non-Cryst. Solids* **2003**, *329*, 1−7.
(30) Mahto, T. K.; Chowdhuri, A. R.; Sahu, S. K. Polyaniline-Functionalized Magnetic Nanoparticles for the Removal of Toxic Dye from Wastewater. *J. Appl. Polym. Sci.* **2014**, *131*, 40840.
(31) Li, L.; Fan, L.; Duan, H.; Wang, X.; Luo, C. Magnetically Separable Functionalized Graphene oxide Decorated with Magnetic Cyclodextrin as an Excellent Adsorbent for dye Removal. *RSC Adv.* **2014**, *4*, 37114−37121.
(32) Du, Y.; Pei, M.; He, Y.; Yu, F.; Guo, W.; Wang, L. Preparation, Characterization and Application of Magnetic Fe_3O_4-CS for the Adsorption of Orange I from Aqueous Solutions. *PLoS One* **2014**, *9*, e108647.
(33) Geng, Z.; Lin, Y.; Yu, X.; Shen, Q.; Ma, L.; Li, Z.; Pan, N.; Wang, X. Highly Efficient Dye Adsorption and Removal: A Functional Hybrid of Reduced Graphene Oxide-Fe_3O_4 Nanoparticles as an Easily Regenerative Adsorbent. *J. Mater. Chem.* **2012**, *22*, 3527−3535.
(34) Gunawan, P.; Guan, C.; Song, X.; Zhang, Q.; Leong, S. S. J.; Tang, C.; Chen, Y.; Chan-Park, M. B.; Chang, M. W.; Wang, K.; Xu, R. Hollow Fiber Membrane Decorated with Ag/MWNTs: Toward Effective Water Disinfection and Biofouling Control. *ACS Nano* **2011**, *5*, 10033−10040.
(35) Alito, C. L.; Gunsch, C. K. Assessing the Effects of Silver Nanoparticles on Biological Nutrient Removal in Bench-Scale Activated Sludge Sequencing Batch Reactors. *Environ. Sci. Technol.* **2014**, *48*, 970−976.

DOI: 10.1021/acssuschemeng.5b00577
ACS Sustainable Chem. Eng. 2015, 3, 2291−2302

(36) Dankovich, T. A. Microwave-Assisted Incorporation of Silver Nanoparticles in Paper for Point-of-Use Water Purification. *Environ. Sci.: Nano* **2014**, *1*, 367−378.
(37) Dahl, J. A.; Maddux, B. L. S.; Hutchison, J. E. Toward Greener Nanosynthesis. *Chem. Rev.* **2007**, *107*, 2228−2269.
(38) Hui, C.; Shen, C.; Yang, T.; Bao, L.; Tian, J.; Ding, H.; Li, C.; Gao, H.-J. Large-Scale Fe_3O_4 Nanoparticles Soluble in Water Synthesized by a Facile Method. *J. Phys. Chem. C* **2008**, *112*, 11336−11339.
(39) Roy, S.; Panpalia, S. G.; Nandy, B. C.; Rai, V. K.; Tyagi, L. K.; Dey, S.; Meena, K. C. Effect of Method of Preparation on Chitosan Microspheres of Mefenamic Acid. *Int. J. Pharma. Sci. Drug Res.* **2009**, *1*, 36−42.
(40) Zhu, J.; Wang, Y.; Liu, J.; Zhang, Y. Facil One-Pot Synthesis of Novel Sperical Zeolite-Reduced Graphene Oxide Composites for Cationic Dye Adsorption. *Ind. Eng. Chem. Res.* **2014**, *53*, 13711−13717.
(41) Das, S. K.; Shome, I.; Guha, A. K. Biotechnological Potential of Soil Isolate, *Flavobacterium mizutaii* for Removal of Azo Dyes: Kinetics, Isotherm, and Microscopic Study. *Sep. Sci. Technol.* **2012**, *47*, 1913−1925.
(42) Sun, H.; Gao, N.; Ren, K. D. J.; Qu, X. Graphene Quantum Dots-Band-Aids Used for Wound Disinfection. *ACS Nano* **2014**, *8*, 6202−6210.
(43) Liu, Z.; Wang, H.; Liu, C.; Jiang, Y.; Yu, G.; Mu, X.; Wang, X. Magnetic Cellulose-Chitosan Hydrogels Prepared from Ionic Liquids as Reusable Adsorbent for Removal of Heavy Metal Ions. *Chem. Commun.* **2012**, *48*, 7350−7352.
(44) Zhu, M.; Diao, G. Synthesis of Porous Fe_3O_4 Nanospheres and Its Application for the Catalytic Degradation of Xylenol Orange. *J. Phys. Chem. C* **2011**, *115*, 18923−18934.
(45) Yin, Y.; Liu, J.; Jiang, G. Sunlight-Induced Reduction of Ionic Ag and Au to Metallic Nanoparticles by Dissolved Organic Matter. *ACS Nano* **2012**, *6*, 7910−7919.
(46) Das, S. K.; Khan, M. M. R.; Guha, A. K.; Das, A. R.; Mandal, A. B. Silver-nano biohybride material: Synthesis, Characterization and Application in Water Purification. *Bioresour. Technol.* **2012**, *124*, 495−499.
(47) Ma, Z.; Guan, Y.; Liu, H. Synthesis and Characterization of Micron-Sized Monodisperse Superparamagnetic Polymer Particles with Amino Groups. *J. Polym. Sci., Part A: Polym. Chem.* **2005**, *43*, 3433−3439.
(48) Lu, C.; Bhatt, L. R.; Jun, H. Y.; Park, S. H.; Chai, K. Y. Carboxyl−Polyethylene Glycol−Phosphoric Acid: A Ligand for Lighly Stabilized Iron Oxide Nanoparticles. *J. Mater. Chem.* **2012**, *22*, 19806−19811.
(49) Zhou, Y.; Yang, D.; Chen, X.; Xu, Q.; Lu, F.; Nie, J. Electrospun Water-Soluble Carboxyethyl Chitosan/Poly(vinyl alcohol) Nanofibrous Membrane as Potential Wound Dressing for Skin Regeneration. *Biomacromolecules* **2008**, *9*, 349−354.
(50) Das, S. K.; Parandhaman, T.; Pentela, N.; Islam, A. K. M. M.; Mandal, A. B.; Mukherjee, M. Understanding the Biosynthesis and Catalytic Activity of Pd, Pt and Ag Nanoparticles in Hydrogenation and Suzuki Coupling Reactions. *J. Phys. Chem. C* **2014**, *118*, 24623−24632.
(51) Duan, B.; Liu, F.; He, M.; Zhang, L. Ag-Fe_3O_4 Nanocomposites@Chitin Microspheres Constructed by In Situ One-pot Synthesis for Rapid Hydrogenation Catalysis. *Green Chem.* **2014**, *16*, 2835−2845.
(52) Liu, Y.-M.; Ju, X.-J.; Xin, Y.; Zheng, W.-C.; Wang, W.; Wei, J.; Xie, R.; Liu, Z.; Chu, L.-Y. A Novel Smart Microsphere with Magnetic Core and Ion-Recognizable Shell for Pb^{2+} Adsorption and Separation. *ACS Appl. Mater. Interfaces* **2014**, *6*, 9530−9542.
(53) Hai, N. H.; Luong, N. H.; Chau, N.; Tai, N. Q. Preparation of Magnetic Nanoparticles Embedded in Polystyrene Microspheres. *J. Phys.: Conf. Ser.* **2009**, *187*, 012009.
(54) Lewandowska, K. Miscibility and Thermal Stability of Poly(Vinyl Alcohol)/Chitosan Mixtures. *Thermochim. Acta* **2009**, *493*, 42−48.
(55) Tripathi, S.; Mehrotra, G. K.; Dutta, P. K. Preparation and Physicochemical Evaluation of Chitosan/Poly(Vinyl Alcohol)/Pectin Ternary Film for Food-Packaging Applications. *Carbohydr. Polym.* **2010**, *79*, 711−716.
(56) Yang, J. M.; Su, W. Y.; Leu, T. L.; Yang, M. C. Evaluation of Chitosan/PVA Blended Hydrogel Membranes. *J. Membr. Sci.* **2004**, *236*, 39−51.
(57) Saha, B.; Das, S.; Saikia, J.; Das, J. Preferential and Enhanced Adsorption of Different Dyes on Iron Oxide Nanoparticles: A Comparative Study. *J. Phys. Chem. C* **2011**, *115*, 8024−8033.
(58) Tomic, N. M.; Dohcevic-Mitrovic, Z. D.; Paunovic, N. M.; Mijin, D. Z.; Radic, N. D.; Grbic, B. V.; Askrabic, S. M.; Babic, B. M.; Bajuk-Bogdanovic, D. V. Nanocrystalline $CeO_{2-\delta}$ as Effective Adsorbent of Azo Dyes. *Langmuir* **2014**, *30*, 11582−11590.
(59) Malik, P. K. Use of Activated Carbons Prepared from Sawdust and Rice-husk for Adsorption of Acid Dyes: A Case Study of Acid Yellow 36. *Dyes Pigm.* **2003**, *56*, 239−249.
(60) Sreelatha, G.; Ageetha, V.; Parmar, J.; Padmaja, P. Equilibrium and Kinetic Studies on Reactive Dye Adsorption Using Palm Shell Powder (An Agrowaste) and Chitosan. *J. Chem. Eng. Data* **2011**, *56*, 35−42.
(61) Sahin, O.; Saka, C.; Kutluay, S. Cold Plasma and Microwave Radiation Applications on Almond Shell Surface and Its Effects on The Adsorption of Eriochrome Black T. *J. Ind. Eng. Chem.* **2013**, *19*, 1617−1623.
(62) Moeinpour, F.; Alimoradi, A.; Kazemi, M. Efficient Removal of Eriochrome Black-T from Aqueous Solution Using $NiFe_2O_4$ Magnetic Nanoparticles. *J. Environ. Health Sci. Eng.* **2014**, *12*, 112.
(63) Ghaedi, M.; Khajesharifi, H.; Yadkuri, A. H.; Roosta, M.; Sahraei, R.; Daneshfar, A. Cadmium Hydroxide Nanowire Loaded on Activated Carbon as Efficient Adsorbent for Removal of Bromocresol Green. *Spectrochim. Acta, Part A* **2012**, *86*, 62−68.
(64) Njoku, V. O.; Foo, K. Y.; Asif, M.; Hameed, B. H. Preparation of Activated Carbons from Rambutan (Nephelium lappaceum) Peel by Microwave-Induced KOH Activation for Acid Yellow 17 Dye Adsorption. *Chem. Eng. J.* **2014**, *250*, 198−204.
(65) Namasivayam, C.; Kavitha, D. Removal of Congo Red from Water by Adsorption onto Activated Carbon Prepared from Coir Pith, an Agricultural Solid Waste. *Dyes Pigm.* **2002**, *54*, 47−58.

DOI: 10.1021/acssuschemeng.5b00577
ACS Sustainable Chem. Eng. 2015, 3, 2291−2302